Using Machine Learning to Predict Optimal Electromagnetic Induction Instrument Configurations for Characterizing the Shallow Subsurface

5   Kim Madsen van't Veen[a], Poul Andrew Ty Ferré[b], Bo Vangsø Iversen[a], Christen Duus Børgesen[a]

[a] Department of Agroecology, Aarhus University, Blichers Allé 20, 8830 Tjele, Denmark
[b] Department of Hydrology and Atmospheric Science, University of Arizona, Tucson, AZ 85721.

10   **Correspondence:** Kim M. van't Veen (km@agro.au.dk)

Abstract. Electromagnetic induction (EMI) is used widely for hydrological and other environmental studies. The apparent electrical conductivity (EC_a), which can be mapped efficiently with EMI, correlates with a variety of important soil attributes. EMI instruments exist with several configurations of coil spacing, orientation, and height. There are general, rule-of-thumb guides to choose an optimal instrument configuration for a specific survey. The goal of this study was to provide a robust and efficient way to design this optimization task. In this investigation, we used machine learning as an efficient tool for interpolating among the results of many forward model runs. Specifically, we generated an ensemble of 100,000 EMI forward models representing the responses of many EMI configurations to a range of three-layer subsurface models. We split the results into training and testing subsets and trained a decision tree (DT) with gradient boosting (GB) to predict the subsurface properties (layer thicknesses and EC values). We further examined the value of prior knowledge that could limit the ranges of some of the soil model parameters. We made use of the intrinsic feature importance measures of machine learning algorithms to identify optimal EMI designs for specific subsurface parameters. The optimal designs identified using this approach agreed with those that are generally recognized as optimal by informed experts for standard survey goals, giving confidence in the ML-based approach. The approach also offered insight that would be difficult if not impossible to offer based on rule-of-thumb optimization. We contend that such ML-informed design approaches could be applied broadly to other survey design challenges.

1 Introduction

Water movement through the vadose zone is often controlled by the near surface layering of soil. In the simplest sense, this is often represented as a small number of horizontal layers, such as is often related to soil formation processes leading to distinct

30 soil layers. The hydrogeologic structure places critical controls on processes ranging from infiltration to percolation to root water uptake to recharge, thereby playing a critical role in most hydrologic systems (Winter et al., 1998; Nimmo, 2009). The need to describe this shallow hydrogeologic structure has been a major driver in the development and adoption of hydrogeophysical methods (Binley et al., 2015).

35 Electromagnetic induction (EMI) is a non-contact method to measure the apparent electrical conductivity (EC_a) of the shallow subsurface. The EC_a is an integration of the electrical conductivity of all layers in the subsurface. EMI works when a transmitter coil produces an electromagnetic field that induces secondary currents in the subsurface soils. The combined current is measured with a receiver coil (Nabighian and Macnae, 1991). The strength of the measured field is used to estimate the EC_a within the sample volume of the measurement (Doolittle and Brevik, 2014). EMI instruments differ in the orientations of their
40 coils: some use transmitter and receiver coils that have their long axis horizontal with respect to the ground surface (HCP), others orient both coils vertically (VCP), and some use one horizontal and one vertical coil in a perpendicular arrangement (PRP). In addition, instruments differ in the separation of the coils, with larger separations used to measure to greater depth. Finally, an operator can choose different instrument heights above ground, which also impacts the spatial sensitivity of the measurement in the subsurface. We refer to the collective choices of coil orientation, separation, and height above ground as
45 the instrument configuration.

For several decades, EMI instruments have been used to gather measurements of EC_a of the soil. The EC_a of soil is positively correlated with salinity, water content, and clay content (Doolittle and Brevik, 2014). As a result, EC_a is a meaningful, but complex, aggregate measure of soil properties (Palacky, 2011). Because the EMI method is non-contact, it is reasonably fast and inexpensive compared to direct soil sampling, resulting in a frequent use in agriculture (McCutcheon et al., 2006; Daccache
50 et al, 2015; Adhikari and Hartemink, 2017), soil mapping (James et al., 2003; Cockx et al., 2009; Heil and Schmidhalter, 2012; Reyes et al., 2018), and archaeological investigations (Saey et al., 2013; De Smedt et al., 2014; Saey et al., 2015; Christiansen et al., 2016). In addition to the challenges introduced by EC_a being sensitive to multiple soil properties, quantitative interpretation of EMI measurements is complicated by the complex averaging of the local soil EC within the instrument's sample volume. (Note that we use the term EC to refer to the actual bulk electrical conductivity of a soil, which may vary
55 within the measurement volume of the instrument, and EC_a to refer to the average EC that is measured from EMI instrument responses.) More challenging still, the spatial sensitivity (or spatial weighting) of the EC depends on the instrument configuration (McNeill, 1980). Finally, in some cases, the spatial sensitivity may have a higher dependency on the absolute value and spatial distribution of the EC (Callegary et al., 2012). In this investigation, we avoid the common assumption that the spatial sensitivity only depends on the instrument configuration, but consider a complete forward model of EMI response.
60 The spatial averaging of EMI is not an issue if the medium is electrically homogeneous. However, most soils have some structure – at a minimum, agricultural soils display horizontal layering with a distinct uppermost layer (the Ap horizon). Therefore, optimal design of an EMI configuration should select the orientation, separation, and height of the coils to locate the instrument sensitivity in the subsurface to best determine the subsurface properties. The depth of investigation (DOI) of

2

EMI instruments is both in the scientific literature (Saey et al., 2009a; Saey et al., 2009b; Saey et al., 2012; De Smedt et al., 2014; Doolittle & Brevik, 2014; Adamchuk et al., 2015) and by the manufacturers (Dualem Inc., Canada n.d.) often estimated to be at the depth the has 70% of the cumulative response. There is a relationship between depth sensitivity of the instrument response and coil spacing and position. Therefore 70% cumulative response rule is in practice frequently converted to a rule of thumb that states larger coil spacings and HCP should be used for deeper investigations while short spacing and VCP/PRP should be used for shallow investigation (Acworth, 1999; Beamish, 2011; Cockx et al., 2009; K Heil & Schmidhalter, 2015; Kurt Heil & Schmidhalter, 2019). While this rule of thumb is not wrong, the terms shallow and deep are subjective and will have different meaning depending on whether it is a hydrogeologist, archeologist, agronomist or a geophysicist who applies the terms. It also fails to make any distinction to the differences between using the VCP or PRP coil orientation. These basic guides become more difficult if the objective is to determine subsurface properties in a non-homogeneous medium, even a simple layered case. For these conditions, the advice is to use multiple coils with some combination of orientation, separation, and height. Nevertheless, little specific guidance is offered. Furthermore, the rule of thumb offers no way to consider the possible impact of prior knowledge (e.g., bounds on the expected depth of the topmost layer) in the survey design. Commercially available EMI instruments for relatively shallow applications offer a wide range of designs based on differences in the three instrument characteristics. This makes it difficult to make an informed choice regarding the preferred instrument and configuration.

Aside from the generally applied rule of thumb and sensitivity analysis there are several published efforts to optimize the design of geophysical surveys (e.g. Furman et al., 2007; Khodja et al., 2010; Song et al., 2016). These methods seek to estimate the reduction in prediction uncertainty based on changes in experiment design through inverse modelling. Applying these design optimization approaches to EMI would require that the responses of many configurations be computed for multiple soil models. Each survey design includes multiple measurements at each location, each with a different configuration, that jointly provide the most useful information for inferring specific, user-identified subsurface properties. That is, a user is faced with the question of which *combination* of configurations is optimal given their measurement priorities and, ideally, incorporating any applicable constraints that they may have regarding the subsurface conditions. Any method that requires formal inversion of each proposed combination of configurations is computationally expensive.

Machine Learning (ML) describes a wide range of regression algorithms used for pattern recognition. ML has grown in popularity and is now used regularly within and beyond science. The simplest ML tools are based on Decision Trees (DT), which are supervised ML techniques that perform classification or regression based on observations. DTs are computationally inexpensive, but they can have limited predictive skill (Hastie et al., 2001). To improve their performance, DTs are often augmented by ensemble learning methods such as bagging (Breiman, 1996) and boosting (Friedman, 2001). The ML approach is different than traditional inverse modelling because the ML is trained to balance generalization with goodness of fit. A sensitivity or inverse model approach would have to be repeated multiple times for each subset to estimate the value of every instrument configuration. The feature importance of tree-based ML gives a data value analysis at each step of the ML training

procedure without extra effort. This makes the ML approach very efficient for calculating the information content of instrument configurations for an ensemble of soils compared to the inverse analysis of data value.

100 One of the challenges of both scientific and environmental investigations is to determine the optimal data to acquire. Data, which is often used to either provide structural information or constrain model parameterization. Measurement optimization is an attempt to balance data quality and the work expended in the field and laboratory. The ultimate goal is to develop an efficient and robust approach to measurement optimization, with the hope that a similar approach could be extended into other measurement network design problems. The specific objective of this investigation was to present the approach in combination

105 with a simple geophysical model to select sets of EMI configurations that are optimal given the specific survey goals and any independent knowledge of the subsurface electrical properties.

2 Theory

2.1 Depth sensitivity of EMI instruments

If the subsurface is electrically homogeneous within the sample volume of the instrument, then the EMI instrument response

110 (EC$_a$) can be related directly to the EC of the subsurface. In almost all subsurface media the EC varies with depth due to soil layering. For these conditions, multiple measurements, made using different coil spacing and separations, can be interpreted simultaneously to infer the EC profile. This requires a model of the depth sensitivity of the EMI measurement.

We apply the Maxwell-based full solutions (eq. 1, 2 and 3) from Wait (1982) to calculate the relationship Q between the secondary field (H$_s$) and the primary field (H$_p$). The solution works for a one-dimensional subsurface and it is valid for low

115 frequencies because it assumes that the electromagnetic fields spread due to conduction currents:

$$Q_{VCP} = Im\left(\frac{H_S}{H_P}\right)_{VCP} = Im\left(-s^2 \int_0^\infty R_0 J_1(s\lambda)\lambda d\lambda\right), \tag{1}$$

$$Q_{HCP} = Im\left(\frac{H_S}{H_P}\right)_{HCP} = Im\left(-s^3 \int_0^\infty R_0 J_0(s\lambda)\lambda^2 d\lambda\right), \tag{2}$$

$$Q_{PRP} = Im\left(\frac{H_S}{H_P}\right)_{PRP} = Im\left(-s^3 \int_0^\infty R_0 J_1(s\lambda)\lambda^2 d\lambda\right), \tag{3}$$

120 Where Im means that only the imaginary component is considered, R_0 is an interlayer reflection factor, J_0 and J_1 are Bessel functions of respectively zeroth and first orders and λ is the radial wave number. The integrals of eq. 1, 2 and 3 represent Hankel transform and in the EMagPy software (McLachlan et al., 2020) these are calculated with linear filtering (Anderson, 1979; Guptasarma & Singh, 1997). The LIN approximation proposed by McNeil (1980) assumes that depth of investigation does not depend on the EC of the subsurface. Therefore, a method similar to that of von Hebel et al. (2019) is used through

125 EMagPy (McLachlan et al., 2020) to estimate EC$_a$ from Q. The EC$_a$ is estimated by minimizing the differences between a predicted or measured Q$_{pred}$ and a Q value calculated for an equal homogenous half-space, Q$_{homo}$. The minimized difference

approach is valid for a broader range of EC_a compared to the LIN approximation (Von Hebel et al., 2019; McLachlan et al., 2020). We refer to Von Hebel et al. (2019) for a more detailed description of this method.

Many efforts have been made to create geophysical modelling tools (Monteiro Santos 2004; Auken et al., 2015; Saey et al., 2016). However, EMagPy (McLachlan et al., 2020) offers the user the opportunity to use several models and makes them readily available to a wide audience, because it is an open source software. This study uses a complete forward model when estimating EC_a, but there is no hindrance to use a simpler geophysical model or a model describing a different process.

3 Materials and Methods

In this study, we describe a specific EMI instrument configuration based on the three coil orientations horizontal (HCP), vertical (VCP), perpendicular (PRP), coil separation (in m), and instrument height (in m). For example, a configuration that uses coils that are horizontal to the surface with a separation of 1 m and an instrument height of 0.3 m would be named: hcp_1.0_0.3. The EC of any layer is an actual electrical property of that specific medium and it is referred to as EC followed by the layer name. For example, the EC of the A-layer is referred to as ECA. Likewise, the thickness of any layer is denoted by Thick followed by the layer name. Thus, the thickness of the A-layer is denoted as ThickA. All symbols and abbreviations can be found in Appendix A.

3.1 Generating the model ensemble

We consider a three-layer soil profile, which is common for agricultural soils with distinctly developed A-, B- and C-layers characterizing changes in the physical, chemical and biological characteristics with depth (Fig. 1). Electrical properties are assumed to be constant horizontally within the sample volume of the instrument. The subsurface properties (three EC values and two thicknesses) were varied independently (Table 1), forming a large set of subsurface conditions. Then, the EC_a was calculated for many EMI instrument configurations through EMagPy (Mclachlan et al., 2020) version 1.1.0. EMagPy deployed the Q response functions from eq. 1, 2 and 3 (Wait, 1982) in combination minimizing the differences between Q_{pred} and Q_{homo} to estimate EC_a.
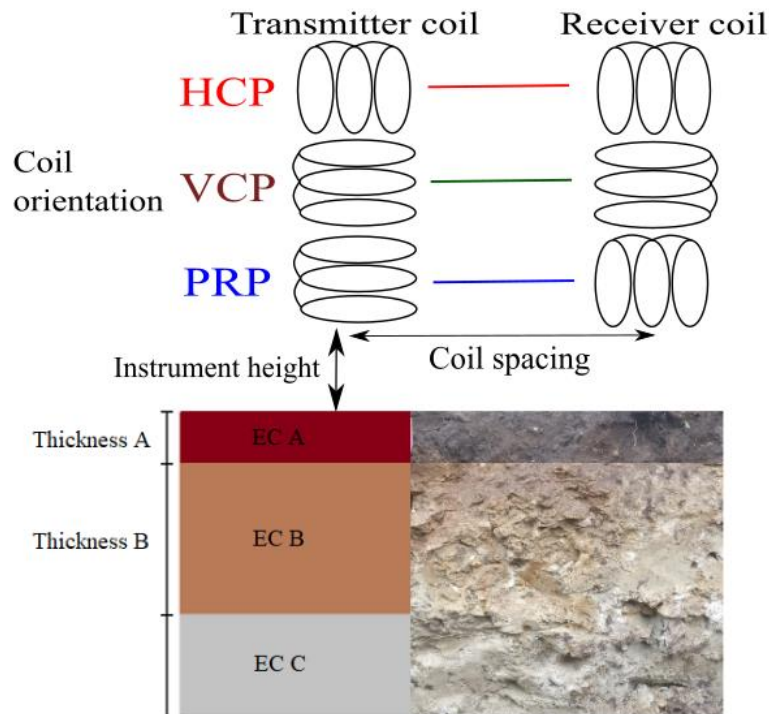
Each of the five soil parameters had ten possible values, which created 100,000 different EC soil profiles. The ranges of EC used in the forward model were chosen to represent a wide spectrum of soil types and water contents. This is to capture different scenarios of EMI use e.g., a survey of a large heterogenous area. The lowest EC represents a dry sandy soil and the highest EC represent an agricultural soil with a combination of high clay or water content (Triantafilis and Lesch, 2005; Robinson et al., 2008; Harvey and Morgan, 2009). The ranges of soil layer thicknesses span from 0.05 m to 2.0 m thickness. The full ranges of the subsurface properties are supposed to cover the range of multiple field sites and we therefore consider a wide range of geology and variation in EC (Palacky, 2011). Each of the three coil orientations was modelled for three different coil separations and three different instrument heights, the 27 instrument configurations cover both the more typical configurations for field applications of EMI and some more uncommon configuration. In total, the EMagPy code was run 2.7 million times to form the ensemble of results covering the soils and instrument configurations.

Table 1: Adjustable parameters used in the forward model to generate the ensemble and values used for each of the combinations that constitute the soil profiles.

Subsurface parameters				
ECA	ThickA	ECB	ThickB	ECC
[mS/m]	[m]	[mS/m]	[m]	[mS/m]
1	0.05	1	0.1	1
12	0.21	12	0.3	12
23	0.37	23	0.5	23
34	0.53	34	0.7	34
45	0.69	45	0.9	45
56	0.86	56	1.1	56
67	1.02	67	1.4	67
78	1.18	78	1.6	78
89	1.34	89	1.8	89
100	1.5	100	2.0	100
Instrument parameters				
Height		Coil spacing		Coil orientation
	m			
0.1		1.0		Vertical
0.3		2.5		Horizontal
0.5		4.0		Perpendicular

3.2 Analyzing the EMI model results and feature importance with a gradient boosted decision tree

3.2.1 Decision tree models

Decision tree is a machine learning method that performs regression or classification practicing on subset of the full data set called training data. A training data set consists of n samples $(x_1, y_1), (x_2, y_2), \ldots, (x_n, y_n)$, where x_{1-n} are the inputs (features) and y_{1-n} are the corresponding outputs (targets). The aim is to estimate a function $F(x)$ that connect the features with the targets in a way that minimizes the loss function (Friedman, 2001):

$$L\big(y, F(x)\big) = \sum_{i=1}^{n} \frac{1}{2} [y_i - F(x_i)]^2, \tag{5}$$

The features in our dataset consists of values of modelled EC_a from various instrument configurations and the targets are the five adjustable subsurface parameters. The tree is built by splitting the values of the features in the training data into two groups. The optimal split minimizes the sum of squared residuals between the value of the targets and the average value of all

180　target within each group. The two new groups are split into additional two groups each (Hastie et al., 2001). This process

continues creating a structure like an upside-down real-world tree with a root node at the top, from which non-terminal nodes

(branches) will be at every split, and terminal nodes (leaves) at every end point. To avoid overfitting the growth of the tree is

limited by introducing a maximum depth of the tree and a minimum number of data samples required to create a leaf by

splitting a non-terminal node.

185

3.2.2 Gradient boosting algorithm

The GB algorithm (Friedman et al., 2001; Mason et al., 1999) takes the training data set and the chosen loss function to make

an initial estimate $F_0(x)$ as a starting point. When the loss function is defined by eq. 5 the initial estimate $F_0(x)$ becomes the

average of the inputs x_1, x_2, …, x_n. The residual r_{im} between the initial estimate calculated by $F_0(x)$ and the true value of the

190　targets are calculated for i=1, 2, …, n:

$$r_{im} - \left[\frac{\partial L(y_i, F(x_i))}{\partial F(x_i)} \right]_{F(x)=F_{m-1}(x)}, \tag{6}$$

Right side of the minus sign in equation 6. is the gradient from which the algorithm is named, and the residual r_{im} are named

pseudo-residuals. Then a decision tree model is made from the features to predict the pseudo-residuals from eq. 6. The decision

tree model output is scaled by a learning rate v to reduce variance of the prediction. The scaled output is added to $F_0(x)$ to

195　create a new function $F_m(x)$ for decision tree m for i=1, 2, …, n:

$$F_m(x) = F_{m-1}(x) + v \sum_{j=1}^{J_m} \gamma_{jm} I(x \in R_{jm}), \tag{7}$$

Where J_m is the total number of leaves in the terminal region R_{jm} in decision tree model m. The new function $F_m(x)$ is used to

calculate a new set of pseudo residuals. The process of making a new decision tree model $F_m(x)$ and adding the scaled output

to the existing function $F_{m-1}(x)$ is repeated until the reduction in pseudo residuals with each added tree becomes insignificant

200　or a specified number of trees M has been created.

Feature importance is an indicator of how valuable each of the included features is in the context of the final decision with

GB. The relative importance $\hat{I}_j^2$ of any feature is proportional to the number of times it is used to make splits weighted by the

square of its improvement to the goodness of fit for the model at each split (Friedman and Meulman, 2003):

$$\hat{I}_j^2(T) = \sum_{t=1}^{J-1} \hat{i}_t^2 1(v_t = j), \tag{8}$$

8

205   which sums over the non-terminal nodes J-1 in the tree T and the squared residual $\hat{\iota}_t^2$ attributed to the split of each node t with

v_t as the target variable being split at each node (Friedman, 2001). Since boosting generates multiple trees the relative

importance is averaged over all trees. The importance is normalized over all features so that the sum of the feature importance

values equals one where a higher value indicates a greater effect on the targets.

210   We found that gradient boosting (Elith et al., 2008; Friedman, 2001) offered improved performance without adding

unreasonable additional computational effort and it was used for all analyses. For our application, each modelled EC_a value in

the ensemble of the different EMI configuration represents a feature in ML parlance. We then tested the ability of DT with GB

to infer the correct value of each subsurface property given the EC_a that would be measured with all the EMI configurations.

A separate boosted tree was trained to predict each of the five subsurface parameters. The EMI model ensemble was split into

215   training and testing sets, with 70% used for training and the remaining 30% used for testing, using the random sample function

in python. Training and testing were repeated five times with different training/testing splits. Differences among the repeats

were small, so all results were combined for analyses. The learning rate, maximum tree depth, and minimum samples per leaf

were tuned by manual trial and error and the optimal values for these parameters were found to be 0.1, 10, and 2, respectively.

However, the performance of the DT with GB did not vary significantly with the hyperparameter values. All other

220   hyperparameters used the default values in the scikit-learn toolbox (Pedregosa et al., 2011).

We used the feature importance capabilities of DT with GB to identify which observed EC_a values were most informative for

the inference and eliminated all insensitive configurations. This allows us to find the optimal instrument configurations for

each subsurface parameter without having to do inverse modelling. To examine the impact of independent knowledge of any

of the subsurface properties, we then repeated this analysis for a subset of the soil models that met a given restriction, such as

225   only those that had a thin upper layer or a high EC middle layer.

3.3 Assessing the value of additional information

For our initial analyses, we considered the full range of all the subsurface electrical properties. However, in many cases, prior

information is available to define one or more of these soil EC parameters or, at least, to reduce the range of plausible values

for at least one of them. This prior knowledge could be in form of hard data or soft expert knowledge for a survey area. This

230   study uses layer EC and thickness as prior knowledge, but any information can be considered to constrain the range of cases.

Here, we examine how reducing the uncertainty of one soil EC parameter improves the EMI-based inference of other parameter

values and whether this additional information changes the composition of the optimal EMI configurations to include in a

survey. Additionally, to the sensitivity of the configurations this analysis provides the parameter values that results in

significantly lowered identifiability of any one of the five subsurface parameters.

235   To examine the value of additional a-priori parameter information, we perform three restriction analyses. In each case, we

sequentially limit the range of one of the five subsurface EC parameters and determine the impact on the accuracy of inference

of the other parameters. Recognizing that some parameters, especially EC values, can have a different impact on EMI spatial sensitivity if they are high or low valued, we consider four patterns of restriction:

- Centered: The four minimum and four maximum values defining the parameter ranges are eliminated.
- Skew low: The eight highest values are eliminated from the parameter range.
- Skew high: The eight lowest values are eliminated from the parameter range.
- Full range: All ten possible values of the five parameters are used in the analysis.

For each restriction analysis, we present the impact of the restriction compared to the case with no independent information and we describe any changes in the composition of the optimal EMI configuration set for each target subsurface parameter.

4 Results and discussion

In this section, we present the outcome from the forward modelling with the full solutions for VCP (eq. 1), HCP (eq. 2) and PRP (eq. 3) and the summation from eq. 4 (section 4.1). We also assess the results from applying a DT with GB to output of the forward modelling. First, we look at parameter identifiability and examine the cases that lead to inaccurate predictions (section 4.2) and then we examine the feature importance output (section 4.3). We show the impact of restricting the range of ThickA on inferring ECA (section 4.4.1). Analysis described in sections 4.1 to 4.4.1 focuses on the full range of parameters and ECA, the EC of the A-layer (the shallowest layer). Finally, we present the impact of piecewise applying all restriction patterns to all five subsurface parameters on the value of independent information (section 4.4.2) and the feature importance of EMI configurations (section 4.5). The results will be influenced by the choice of forward model, but the ML approach to design optimization is not model dependent and a change in forward model is a trivial extension.

4.1 Modelled EC_a ensemble

The five soil parameters with ten different values provides us with an ensemble of 100,000 soil profiles. The three coil orientations, three coil spacings, and three instrument height sums to 27 instrument designs that are applied to each profile. Frequency distributions of the modelled EC_a for each of the 27 instrument designs in all the profiles are shown in Fig. 2. The distributions are quite similar, but they do differ in detail. The distributions of modelled EC_a values depend strongly on the height or coil orientation for designs with a 1-meter coil separation (left column, Fig. 2). The variations are less pronounced for larger coil separations. There are also differences in the smoothness of the distributions: the PRP (bottom row, Fig. 2) has more distinct peaks for small separations whereas the HCP (top row, Fig. 2) has more peaks for larger separations.
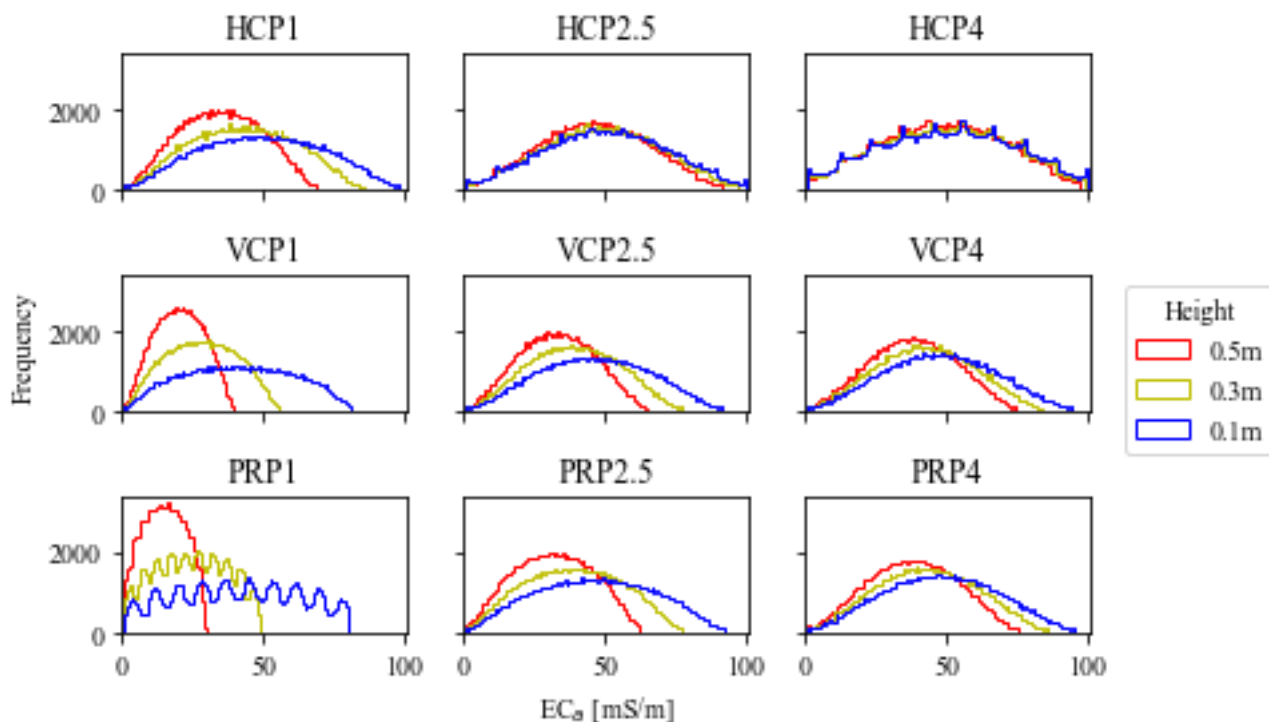
Figure 2: Frequency distributions of the responses from the cumulative sensitivity model for the three coil orientations: Horizontal (HCP), vertical (VCP) and perpendicular (PRP). Each panel shows the modelled EC_a output from one coil orientation and -separation for three different heights. The coil orientation and -separation change respectively with the rows and columns of the nine panels.

4.2 Predicting parameter values with a trained DT with GB using all observations

The first step in our analysis was to examine the ability of the trained DT with GB to predict each parameter value. That is, we use 70,000 EC profile realizations for training the DT with GB. We then provide the 27 observations for each of the remaining 30,000 EC profile realizations to the trained DT with GB and predicted ECA (the EC of the shallowest layer). To account for the brittle nature of DT methods, this procedure was repeated five times with different training/testing splits. The results of the repeated analysis were not significantly different, so they were pooled, providing 150,000 predictions upon which the goodness of fit was determined.

The root mean squared error (RMSE) between predicted and true values of the EC of the A-layer (ECA) is shown on Figure 3. The true values are the known ECA values used in the forward models. The results, shown as a cross-plot of points, are somewhat misleading because it is difficult to see that many points are overlapping close to the 1:1 line. Therefore, shaded areas are included to show ± one and two standard deviations about the mean predicted ECA for each true ECA value. There are clear outliers – cases for which the trained DT with GB did not give an accurate estimate of ECA even considering all 27

11

EMI observations. However, the overall RMSE was 7.34 mS/m over the entire set of 150,000 test cases. The residuals shown in Fig. 3 are not evenly distributed at the low and high values because of the lower and upper boundaries of the input values.
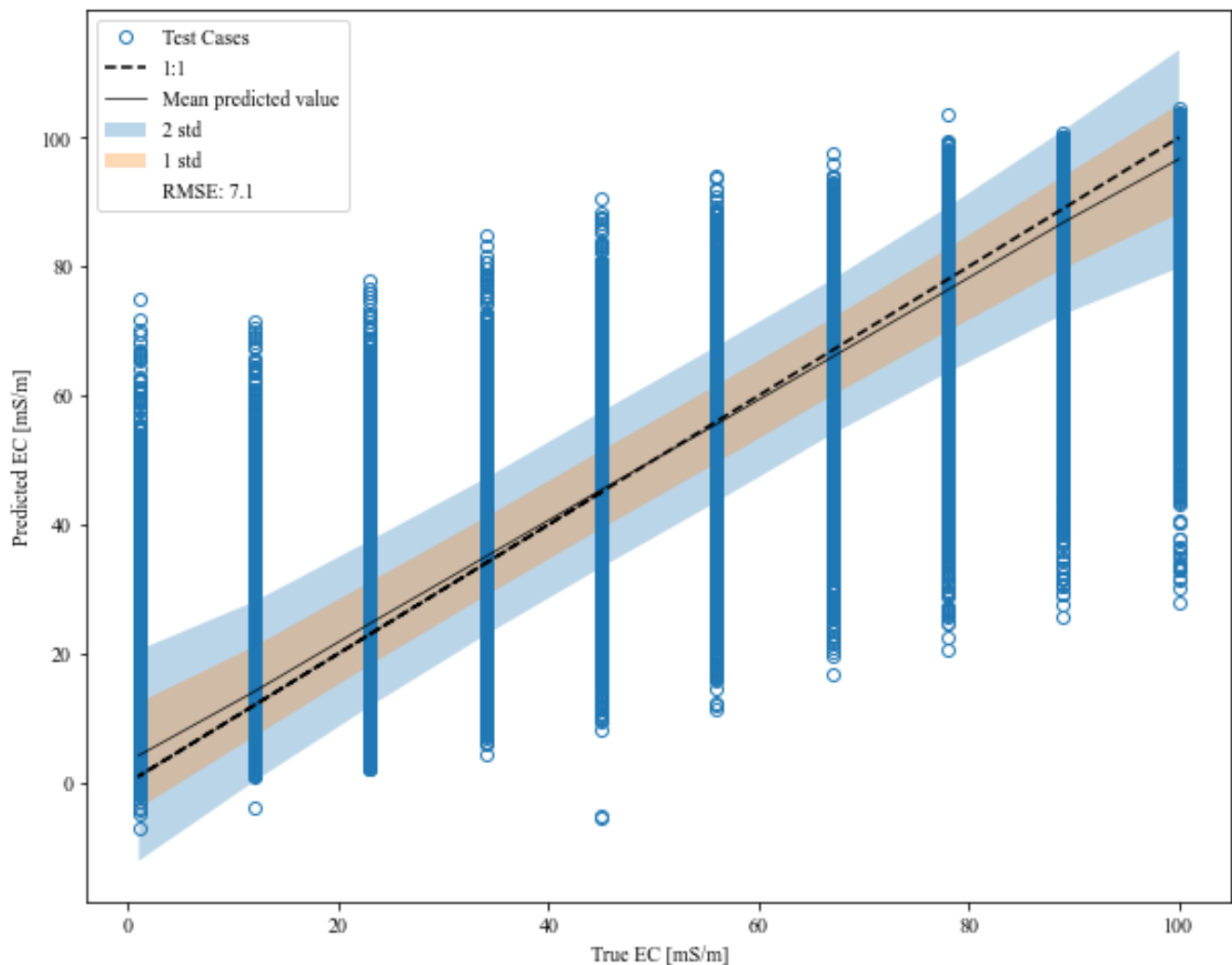
Figure 3: The result from running the DT with GB on the entire 100000 soil types and all 27 instrument configurations five times. The EC of the A-layer (ECA) is the parameter that is being predicted. The X-axis is the true value of the ECA, and the Y-axis is the predicted values for ECA.

The process shown in Fig. 3 was repeated for each of the five EC profile parameters. The RMSE for each parameter is reported in Table 2 and a table of how gaussian noise affect the RMSE is shown in appendix B. Because the range of values of the parameters differ, the normalized root mean square error (NRMSE) is calculated by dividing the RMSE by the full range of the true values of the parameter. The NRMSE of the parameter is a measure of how well the ML can infer the individual parameters and thus how estimable the parameters are. Because the ML is trained on EMI output the NRMSE also suggests

how well the EMI instrument can detect the soil properties. The results show that EMI is least able to infer the layer thicknesses, with slightly better ability to infer the thickness of the A compared to the B-layer. Furthermore, EMI produces better estimates

295   of the shallow and deep EC values compared to the EC of the B-layer. These results fit with expectations, given that EMI designs with very short coil separations might be sensitive to only ECA and those with very large separations might be mostly sensitive to the EC of the deepest layer, ECC (Callegary et al., 2012; Heil and Schmidhalter, 2015). In contrast, the layer thicknesses, ThickA and ThickB, and the EC of the middle layer, ECB, must always be inferred based on multiple measurements.

300   **Table 2: The root mean square error (RMSE) between the prediction from the gradient boosted (GB) model and the testing data. The machine learning procedure was repeated with each of the five subsurface parameters as targets, thus creating five models. The RMSE is normalized by the mean value of the target to get the normalized root mean square error (NRMSE).**

Target	ECA	ThickA	ECB	ThickB	ECC
Unit	mS/m	m	mS/m	m	mS/m
RMSE	7.09	0.29	18.8	0.51	2.98
NRMSE	0.07	0.20	0.19	0.27	0.03

4.2.1 Examining the conditions that led to poor estimations of ECA

305   From the 150,000 test cases, displayed on Fig. 3, 8,816 cases are more than one standard deviation away from the true value when predicting ECA. These cases are displayed in Fig. 3 by the blue markers that are located outside the shaded areas. The compositions of these 8,894 cases are presented as frequency distributions of their parameter values in Fig. 4. The values for ECB, ECC, and ThickB are uniformly distributed, which indicates that no specific values of ECB, ECC or ThickB lead to poor inference of ECA. In contrast, 94% of the problematic conditions have a thickness of the A-layer (ThickA) among the three

310   lowest values. This, again, agrees with expectations that the EC of a thin layer would be more difficult to infer accurately than that of a thicker layer using an EMI instrument. The finding is opposite for ECA; while not as pronounced, the results indicate that the poorly inferred cases tended to have higher ECA values, with 54% of the conditions having the three highest ECA values. This suggests that identifying the layer with EMI instrument would be more likely to be successful if the range of ThickA does not include the lowest values examined here; that is, we would expect improved inference of ECA for centered

315   or high skewed restrictions of ThickA. A more successful survey, based on the ability to infer ECA, would occur if the ECA values tend to be lower. That is, a center or low skewed restriction should show better performance.
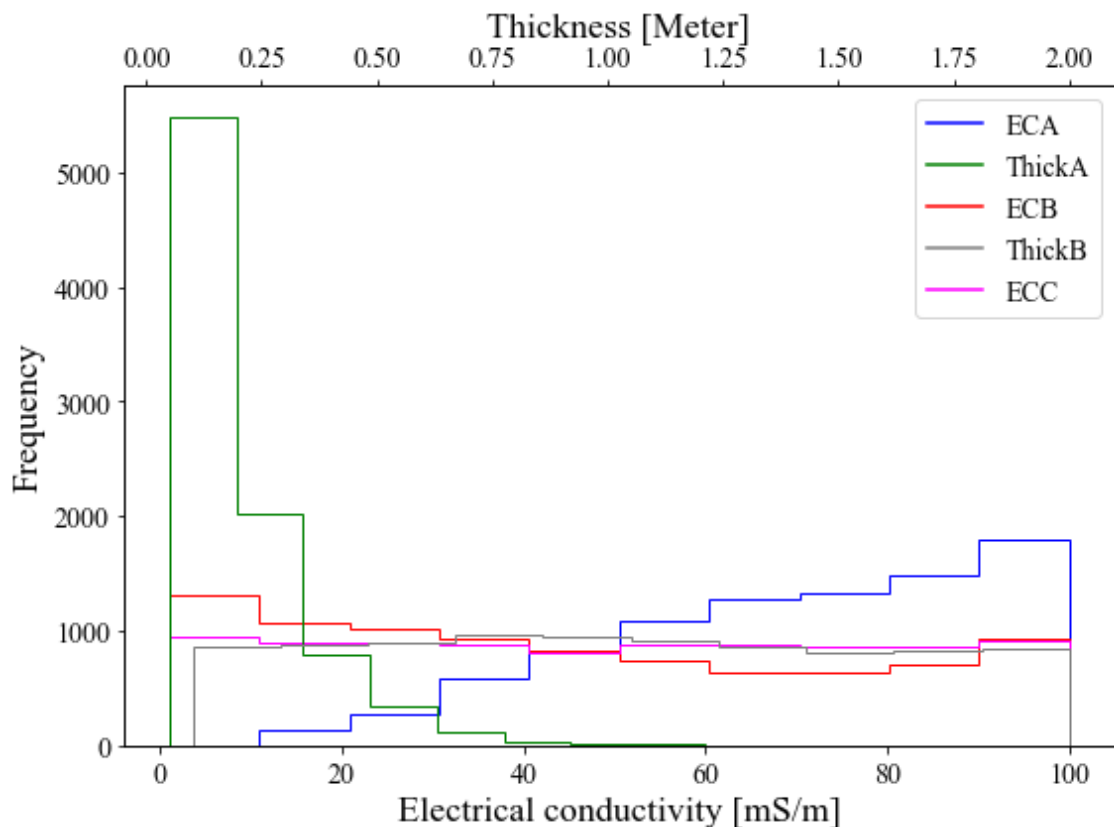
Figure 4: The ECA was inferred for 150,000 test cases. In 8816 of the 150,000 cases the inference was more than one standard deviation away from the true value. The figure shows the distribution of five subsurface parameter values within the 8894 conditions. The top X-axis is the layer thickness, the bottom X-axis is the layer EC and the Y-axis is the frequency.

4.3 Feature importance when predicting parameter values with a trained DT with GB

The preceding analysis used measurements from all 27 instrument configurations for each EC profile parameter estimation. The major focus of this investigation was to use ML tools to identify the optimal set of observations to collect, which balances performance with reduced field effort. To illustrate how the built-in feature importance of tree-based methods can be used to achieve this, consider the results shown on Fig. 5. The feature importance is shown for each of the 27 configurations; because they sum to 1 it is convenient to represent this as a pie chart. The colors and patterns that comprise the circles identify the eight most important EMI configurations for each combination of the parameters. The fraction of the circle covered by each color/pattern shows the relative importance of that observation. The colors indicate the coil orientation, while the shade and pattern indicate the coil distance and instrument height. The 19 least important EMI configurations are combined in "others" (white slices). From these results, it is apparent that approximately 90% of the information used to predict ECC (rightmost

14

circle) is provided by configuration hcp_4.0_0.1. The optimal orientation and large coil separation could have been predicted from McNeil's classic work (McNeill, 1980). However, he did not consider the PRP orientations. The reason for the preference for a small instrument height is as apparent; it may simply be due to further penetration of the signal to greater depth. To our knowledge, no other method, short of exhaustive comparisons of many synthetic inverse analyses, would have been able to

335 show that a single configuration, among the full suite of instruments, was so clearly dominant for inferring ECC. Similarly, almost 60% of the information used to infer ECA (leftmost circle) was provided by the prp_1.0_0.1 configuration. The small coil separation and low instrument height fit with general expectations, the highly sensitive PRP orientation fit with the findings of Tabbagh (1986).


Feature importance for full parameter range
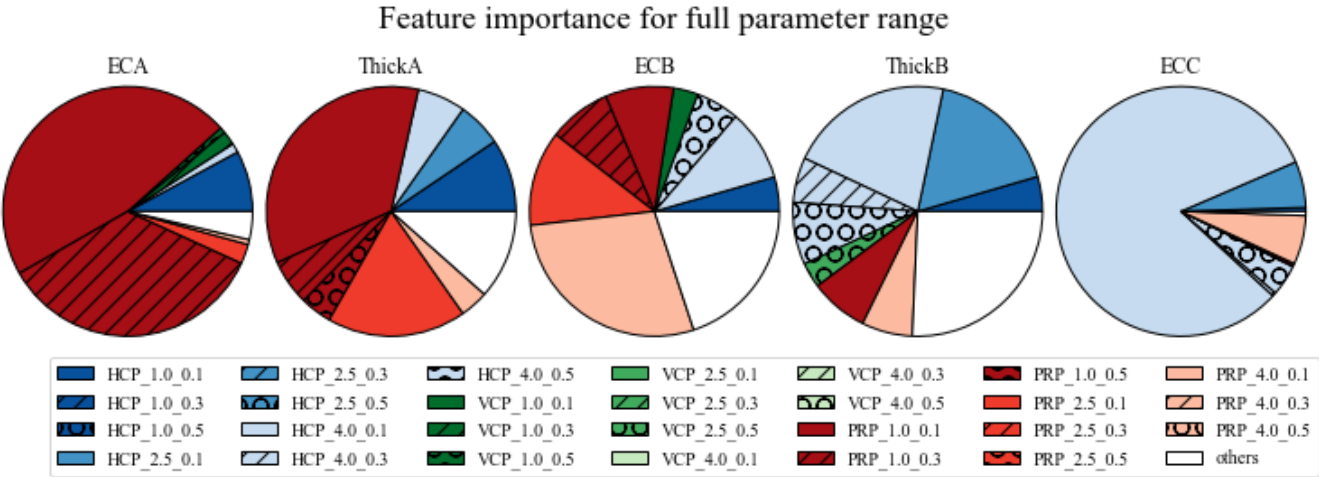
Figure 5: Feature importance for inferring each of the five parameters from a decision tree analysis of the full parameter range. The
340 **feature importance from all 27 configurations sum to 1. The eight most important configurations for inferring each of the five parameters are shown with a unique color and pattern combination. The remaining 19 configurations are aggregated into the "others" category and displayed with white.**

Taken together, the results suggest that each of the EC profile parameters relies on a relatively small number of observations.
345 To illustrate this, 90% of the importance, including only the highest importance observations, is provided by 4, 9, 13, 17, and 3 observation for ECA, ThickA, ECB, ThickB, and ECC, respectively (Fig. 5). Of these high importance observations, 53% had the instrument placed at the lowest instrument height considered. The VCP is the most widely used coil orientation in agriculture (Heil & Schmidhalter, 2017), but it is only 17% of the most informative configurations use the VCP orientation (Fig. 5). This may be explained by the spatial sensitivities of the orientations (Callegary et al., 2007; Christiansen et al., 2016)
350 which indicates the HCP/PRP pairing are more complementary relatively to the HCP/VCP pairing. The influence of simulated noise on the results in Fig. 5 are shown in appendix B.

4.4 Parameter restriction analyses

4.4.1 Applying a skew low restriction to the thickness of layer A

355   One piece of information that may be available (e.g. from direct field examination) is the expected thickness of the shallow topsoil layer (ThickA). Therefore, we begin our restriction analyses by examining the effect of improved knowledge of ThickA on the inference of the ECA parameter. Specifically, we repeated the analysis only including models with the two middle values of ThickA (0.69 m and 0.86 m). This reduces the ThickA parameter range to 11% of its full range and thereby removes the cases that contains low values for ThickA. The results (Fig. 6) show stark improvement in the ability of the DT with GB

360   to infer ECA. A similar analysis could be repeated for any restricted range of value for any parameter or for multiple parameters. This could be done for practical reasons – to design a site-specific survey – or for scientific reasons – to explore which conditions are identifiable with EMI and to understand these parameter interactions.

The analysis leading to Fig. 6 is one example of the ability of the DT with GB method to consider the benefits of independent soil property information. In this section, we expand the investigation to include all the soil electrical parameters and three

365   different restriction patterns.
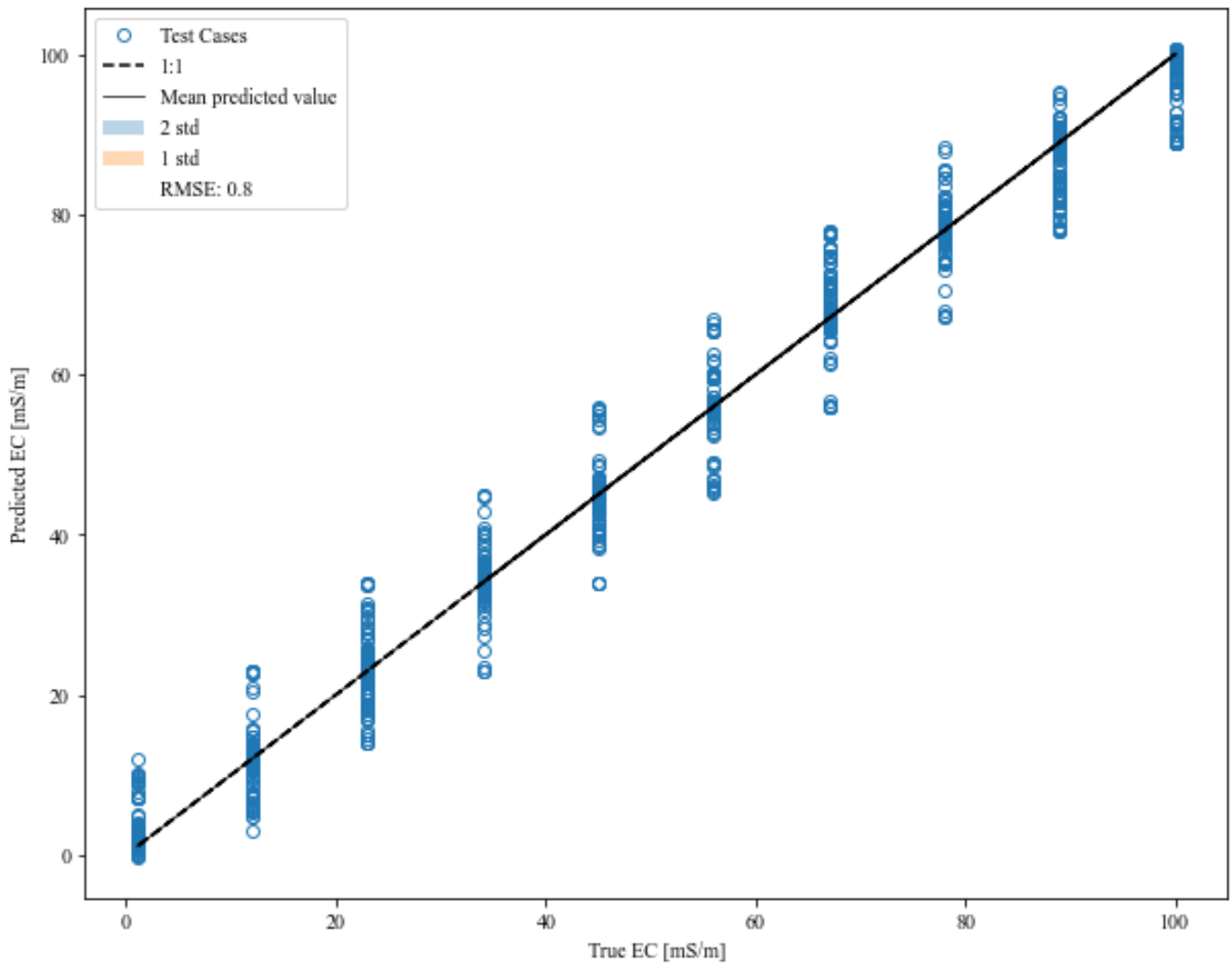
Figure 6: The result from running the machine learning algorithm on a subset of the ensemble where the thickness of the A-layer have been restricted. Only 20,000 soil types and all 27 instrument configurations remain in this restricted subset. The EC of the A-layer (ECA) is the parameter that is being predicted.

4.4.2 Changes in parameter inference of restricted subsets

Figure 7 summarizes the impacts of providing the maximum additional information (considering only two of the ten possible values of one parameter) on the inference of all other parameters. The y-axis on Fig. 7 is the RMSE (such as that reported on Figure 6 for inferring ECA with ThickA restricted) normalized by the full range (max – min) of the inferred parameter. With reference to Fig. 6, this would be reported as the RMSE divided by the range of ECA, giving a unitless value of 0.028. Each inferred parameter is associated with a short horizontal line, which indicates the normalized RMSE without restriction of any other parameter's range. Each symbol on Figure 7 represents the results of an analysis like that shown on Figure 6. There are

17

three symbols (triangle, dot, and square) associated with each target/restricted parameter pair for each of three restriction patterns. Consider, for example, inferring ECA. The set of three blue symbol represents the impact of restricting the range of ECA itself, the leftmost triangle represents skewed low restriction (retaining the two lowest ECA values), the middle dot is a centered restriction (ECA values 45 and 56 mS/m), and the right square represents the skewed high restriction (retaining the two highest ECA values). As expected, restricting the range of ECA, regardless of the restriction pattern, leads to a similar reduction in the normalized RMSE of ECA. Every pair of restricted/inferred parameters is represented using three symbols with the same left nudged triangle, center dot, right nudged square for the low, middle, and high skewed restrictions.

Consider another example to illustrate how Fig. 7 can be interpreted and related to Fig. 6. The three symbols' dots above ECA represent the impact of restricting ThickA. The center dot corresponds exactly to Fig. 6, the centered restriction of ThickA. The left green triangle shows that there is an increase in the NRMSE for the skewed left restriction compared to the unrestricted case (horizontal line above ECA), which shows that restricting the thickness of layer A to the lowest range of values leads to lower quality inference of ECA. In other words, the shallowest layer may be too thin to be detected properly because the instrument response is an integration over a large depth compared to the now relatively thin layer thickness. This fits with previous findings (Fig. 4), which revealed that a thin ThickA makes it difficult to infer ECA. Furthermore, it agrees with our expectations that if the uppermost layer is sufficiently thick, we can choose a coil separation and orientation that is almost exclusively sensitive to the uppermost layer, essentially allowing direct measurement of ECA. Consistent with this explanation, the right green square above ECA has the lowest NRMSE. In this case, this confirms the expectation that it is easier to infer ECA accurately if the shallowest soil layer is relatively thick. Similar interpretations about the value of restricting one parameter on the ability to infer other parameters accurately can be drawn for each pair of restricted/inferred parameters, allowing researchers to gain valuable insight into the interaction of measurements and other independent information. In all cases, there is a reduction in the NRMSE of the inferred parameter when the parameter itself is restricted. For these cases, there are no significant differences among the three restriction patterns. In most cases, restricting the range of the inferred parameter itself showed a greater improvement than restricting any other parameter. The only clear exception was inferring ECA, which showed a greater improvement by restricting ThickA with a central or right skew.
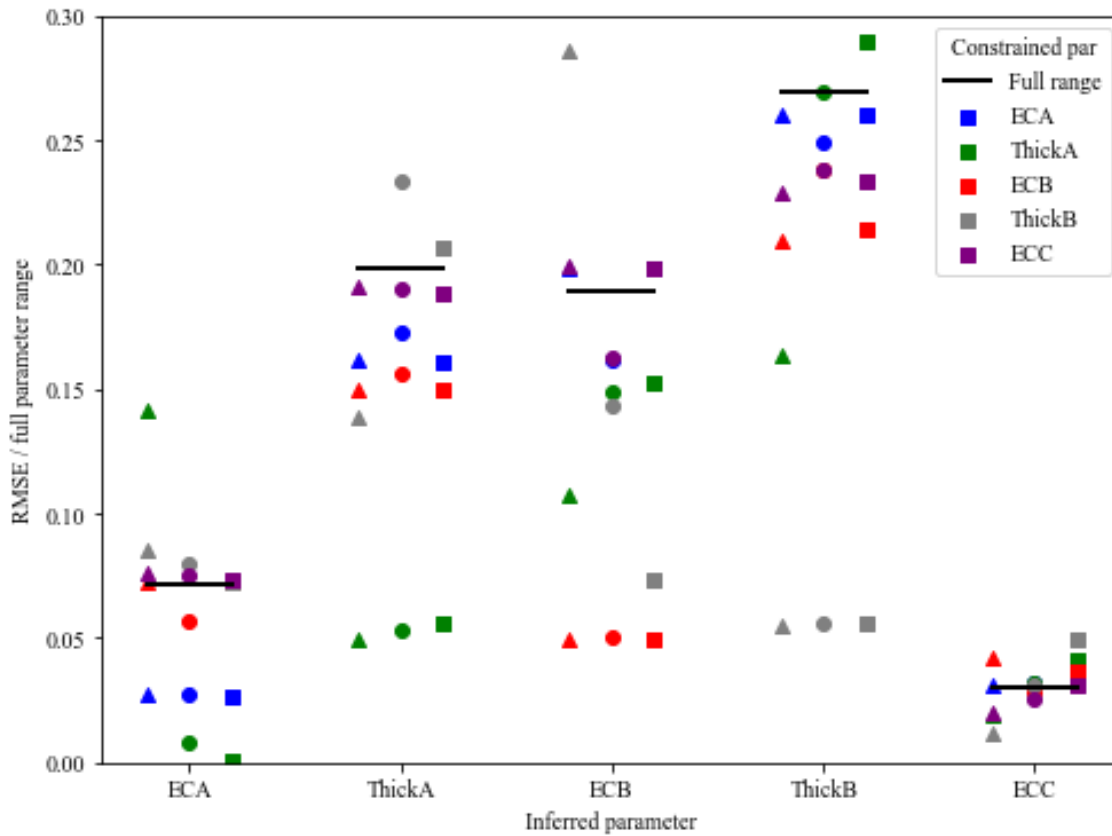
18

Figure 7: The changes in inference of the five subsurface parameters (X-axis) are based on a comparison between the RMSE from restricted case divided by the range of the parameter (Y-axis). The lines show how well the parameters are predicted when all parameters are full range. The color shows which parameter that is being represented and the location and symbol represents the three restriction patterns skewed low (left nudged triangle), centered (centered dot), skewed high (right nudged square).

Consider the inferred parameter ThickB on Fig. 7. The three green symbols represent the cases where ThickA is restricted. The left triangle is the skewed low restriction that results in a reduced NRMSE compared to the full parameter range (black line). The middle dot, which is centered restriction, shows the same NRMSE as the full parameter range. The right square, which is skewed high restriction, has a higher NRMSE than the full parameter range. The changes in NRMSE between the three restrictions of ThickA show that knowledge of the ThickA confers little advantage to estimating ThickB unless it can be shown that the shallowest layer is very thin.

More generally, there are relatively few cases where the restriction of one parameter significantly improves the inference of another parameter. Beneficial restrictions include restricting ECA and ECB to infer ThickA and restricing ThickA and ECA to infer ECB. To a lesser degree restricting any other parameter when inferring ThickB offers a slight advantage. The value of ECC is already well constrained for the full parameter range, as shown by the line, and there is little advantage to restricting another parameter to infer ECC. In 37% of cases, restricting the range of one parameter led to worse inference of another. These cases display the field conditions that lead to more challenging use of EMI, such as a very thin middle layer making it

19

very difficult to infer ECB. An experienced EMI user would be able to reach these conclusions, which helps us to confirm that the ML approach is robust and reaches reasonable results. The value of this type of analysis with a geophysical EMI model is to provide guidance for site-specific conditions, but the analysis can also be executed with more complete geophysical models or different model types. Furthermore, this guidance is quantifiable rather than based on intuition derived from the rule-of-thumb.

4.5 Feature importance in restricted subsets

The composition of the optimal EMI measurement configuration is different depending on the soil layer thicknesses and conductivities. Figure 8 summarizes the feature importance for the cases presented in Figure 7, for which only two out of ten values remain for the restricted parameter. The color and symbol patterns are the same as those used for Fig. 5. The columns in Fig. 8 represent the five inferred parameters and the rows represent the restricted parameter. Consequently, each circle is a pairing between one restricted and one inferred parameter. The circles are subdivided into four rings that represent the different restriction patterns. From inside out, the rings represent the full parameter range (no parameter restriction), centered, skew low, and skew high restriction. The feature importance of the full parameter range (centermost ring) is the same in every row for each inferred parameter. For reference, the center ring results are identical to those presented in Fig. 5. All 75 combinations of the five inferred/restricted parameters and the unrestricted case are shown for the three restriction patterns on Figure 8, allowing a user to draw general insights into the value of different configurations under a wide range of conditions. Fig. 8 is designed to showcase all the different combinations restrictions made to the ensemble in this study but for pure practical application not all combinations would need to be displayed.
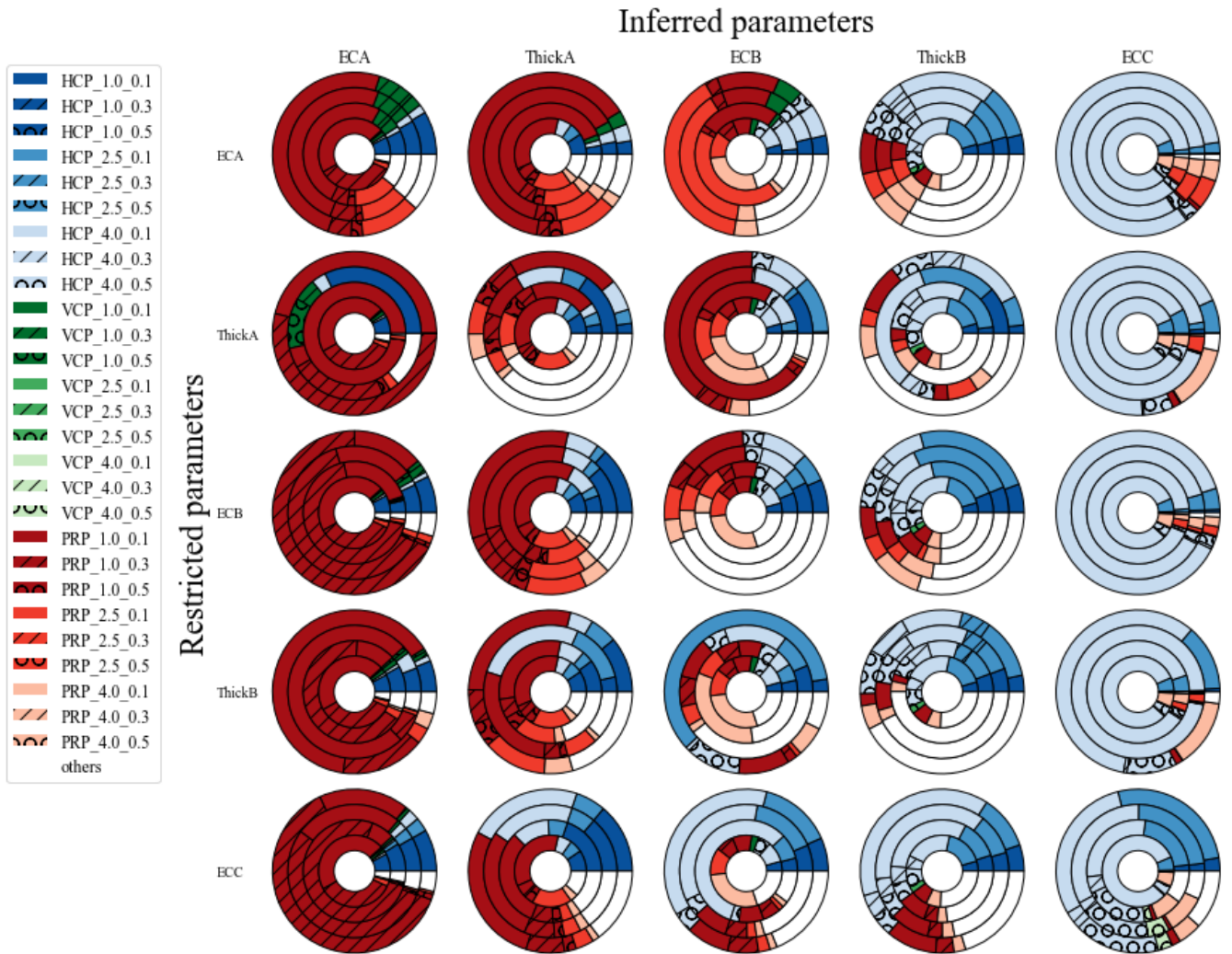
Figure 8: Feature importance for the 8 most important EMI configurations for every combination of the five inferred/restricted parameters and the three patterns. Each circle is subdivided into four rings that shows, from inside out, the feature importance for full range, centered, skew low, and skew high. Each column/row represents the each of the five inferred/restricted parameters. The coil orientations are colored so that Horizontal (HCP) is blue, Vertical (VCP) is green, and Perpendicular (PRP) is red. A dark and light hue represents respectively a short and long coil distance.

Figure 8 is somewhat information dense, so it may be useful to discuss a few cases in more detail. One of the simplest subplots to understand is the inference of ECC when restricting ECA (top right circle). The results show clearly that there is no meaningful change in the composition of the optimal set of configurations due to adding additional ECA information, regardless of the range of ECC values considered: all four concentric rings look nearly identical. Furthermore, all four rings indicate that a single configuration, HCP_4_0.1 provides the vast majority of the information needed to characterize ECC. Again, this is in general agreement with the rules of thumb derived from the 70% rule, but it confirms these findings for all values of EC and thickness of the other layers, and it extends the findings to consider the PRP configuration. Moving down

the ECC column, note the difference when ThickB is restricted. If ThickB is skewed high (ThickB ranges between 1.8 m and

450 2.0 m), there is some advantage to adding the PRP_4_0.1 configuration. Our approach does not explain this choice. We suggest that it is informative to collect this additional observation to constrain the values of ECB and ThickB if the middle layer is relatively thick and that the identified configuration has a usefully different sensitivity distribution than the large HCP array placed close to the ground surface. This result could not be anticipated based on the rule of thumb. Furthermore, the resulting optimal configuration is almost identical if either ThickA or ThickB is restricted, when inferring ECC. Moving to the bottom

455 of that column, the analyses show that if the value of ECC itself is limited then the composition of the optimal set changes significantly. Interestingly, regardless of the pattern of restriction (the results are almost the same for the outer three rings), the optimal set now includes four configurations with approximately equal importance: HCP_4_0.1; HCP_4_0.5; HCP_2.5_0.1; and PRP_4_0.1. It is further confirmation of the validity of the approach that no VCP arrays were chosen, as would be expected based on McNeil (1980). Similarly, as expected, the larger array separations are preferred. It is surprising, however, that one

460 of the four observations place the instrument higher above ground. This is a result of the spatial sensitivities and an example of a conclusions that is very difficult to reach through intuition and the rule-of-thumb. This could point researchers to ask follow-on questions about why a specific configuration or observation type are identified as optimal.

The results for inferring ECA (leftmost column) are similar but show interesting differences. The optimal set for ECA is relatively insensitive to the pattern of restriction of ECA. But more than one observation is required for all cases. Whereas the

465 optimal cases were similar for restricting ThickA and ThickB for inferring ECC, this similarity holds for restricting ECB and ThickB when inferring ECA. The pattern of restriction of ThickA has dramatic impacts on the optimal set of configurations for inferring ECA. Inferring the three other parameters (ThickA, ThickB, and ECB) show significant changes in the optimal configuration set depending upon the pattern of restriction (ring-to-ring) and upon the independent information provided (row-to-row). There is no case for which a single configuration dominates the importance in all rows. In fact, there are many cases

470 that would recommend more than nine configurations. For example, this likely indicates that ThickB is unlikely to be well resolved by a practical field survey. Further considerations of inferring ThickB give interesting general insights compared to rule-of-thumb suggestions. Namely, very few VCP configurations are selected. If PRP arrays are to be used, then profiling should be achieved multiple coil separation pairs with the coil placed close to the ground. For HCP configurations, profiling should be achieved by increasing the coil separation..

475 To summarize, taken together Fig. 7 and 8 provide guidance to an EMI user when designing a survey with a specific target. Figure 7 indicates whether that target can be characterized reliably given the full range of configurations considered and which additional information will improve the characterization. A low NRMSE will suggest a more reliable characterization of the subsurface property by the instrument and vice versa. Figure 8 identifies the optimal set (and number) of arrays needed for optimal characterization. Some of the conclusions would be expected based on the simplified descriptions from McNeil's

480 (1980) classic work and would be anticipated by an experienced EMI user. Other results would be difficult, if not impossible, to predict without a value-of-data analysis like that shown here. These results, in particular, could point the way to further scientific investigations to better understand the complementary information content of multiple EMI configurations. The

restriction analyses offer insight into the mutual identifiability of soil EC. Given the availability and flexibility of EMagPy (Mclachlan et al., 2020) and the efficiency of the DT with GB algorithm, the analyses performed here could be extended to

485 include identification of optimal configuration sets for multiple targets (e.g. thickness and EC of the B layer). For example, placing equal weight on all five targets, an optimal without restriction of any of their values suggests the use of: one HCP array (hcp_4.0_0.1) and four PRP arrays (1.0_0.1, 4.0_0.1, 1.0_0.3, and 2.5_0.1). If this specific set of configurations was deemed impractical, a user could limit the available configurations for consideration, find the optimal survey, and compare the projected RMSE to that estimated for the overall optimal set. This information could guide a user in whether it is worthwhile

490 to change their instruments, or designs, or whether gathering additional information about the range of plausible parameter values is likely to be more important for their survey goals.

In this study 27 instrument configurations in combination with 100000 subsurface models is considered the full ensemble. Using the presented ML approach to assess data value for our full ensemble is more efficient than an inverse (Furman et al., 2007; Khodja et al., 2010; Song et al., 2016) or sensitivity (Hanssens et al., 2019) approach. In some cases, evaluating all

495 instrument configuration will not be necessary, which means the inverse or sensitivity approaches become more efficient. The ML approach requires a certain size of model ensemble to yield stable results therefore model run time will reduce efficiency, but this affects the inverse analysis more because it generally requires more model runs. Ultimately the efficiency of the ML, inverse and sensitivity approaches depends, in the EMI case, on model run time, number of layers, parameter boundaries and the number of considered configuration and the combination of these in the applied case will determine which method is more

500 efficient. Designing a combination of optimal configurations based on a conceptual understanding of the spatial sensitivities (rule of thumb) is not a reasonable task. Furthermore, measurement optimization requires a quantitative measure of the information content. The ML provides a quantitative measure of the shared information among model parameters (Table 2 and Fig. 7) to compare the likely success of each configuration.

Finally, the general approach shown here could be extended easily to consider multiple measurement types (e.g. combining

505 EMI with other geophysical methods), and even dynamic optimization of measurement networks for monitoring applications.

5 Conclusions

Most environmental and agricultural field investigations are conducted on relatively limited budgets. As a result, there is usually some advantage optimizing data collection to achieve the best results with the limited time and money available. These restrictions are one of the main reasons that electromagnetic induction (EMI) has become a popular tool for these studies.

510 While it is often the case that the measurements are more ambiguous than direct measurements of soil properties, the noncontact nature of the instruments allows for much greater spatial coverage. The recent availability of EMagPy (Mclachlan et al., 2020), allowed us to perform the large number of EMI forward models necessary to support a machine learning (ML) examination of EMI surveys, leading to a simple but comprehensive investigation of parameter identifiability and optimal EMI configurations. The result is an approach that can allow an EMI user with limited expertise to choose a better set of instrument

configurations given their main survey goal and knowledge of the site conditions. The same tool can point more advanced users to areas of investigation that may improve our understanding of the prior knowledge content of different EMI configurations. The decision tree with gradient method based on a large ensemble of instrument response forward models, proposed here, makes novel use of the efficiency and built-in feature importance capabilities. But, the analyses are not restricted to this relativley simple ML algorithm. More advanced ML tools could be combined with independent feature importance analyses if required for specific monitoring applications. Similarly, while EMI forward modeling is relatively simple and fast, given that it is based on analytical models, with sufficient computational resources any measurement method and underlying physical process could be examined in the same way. As just one illustrative example, an optimal combination of EMI, electrical resistivity, gravity, and monitoring well observations could be proposed to constrain the interpretation of a pumping test performed in an unconfined, anisotropic medium by conducting forward models of many configurations (survey locations and times, Electrical Resistivity Tomography array types, and screen depths) for a large ensemble of plausible aquifer conditions and allowing an ML algorithm to consider all of the data and identify the most informative observations. This opens the possibilities for exploring truly novel combinations of multimodal observations.

6 Appendices

Appendix A Symbols and abbreviations

CS – Cumulative sensitivity

DT - Decision Trees

EC – Electrical conductivity

EC_a – Apparent electrical conductivity

ECA/B/C – Electrical conductivity of layers A, B and C

EMI – Electromagnetic induction method

GB – Gradient boosting

HCP – Horizontal co-planar

LIN – Low induction number

ML – Machine learning

NRMSE – Normalized root mean square error

PRP – Perpendicular-planar

RMSE – Root mean square error

ThickA/B – Thickness of layers A and B
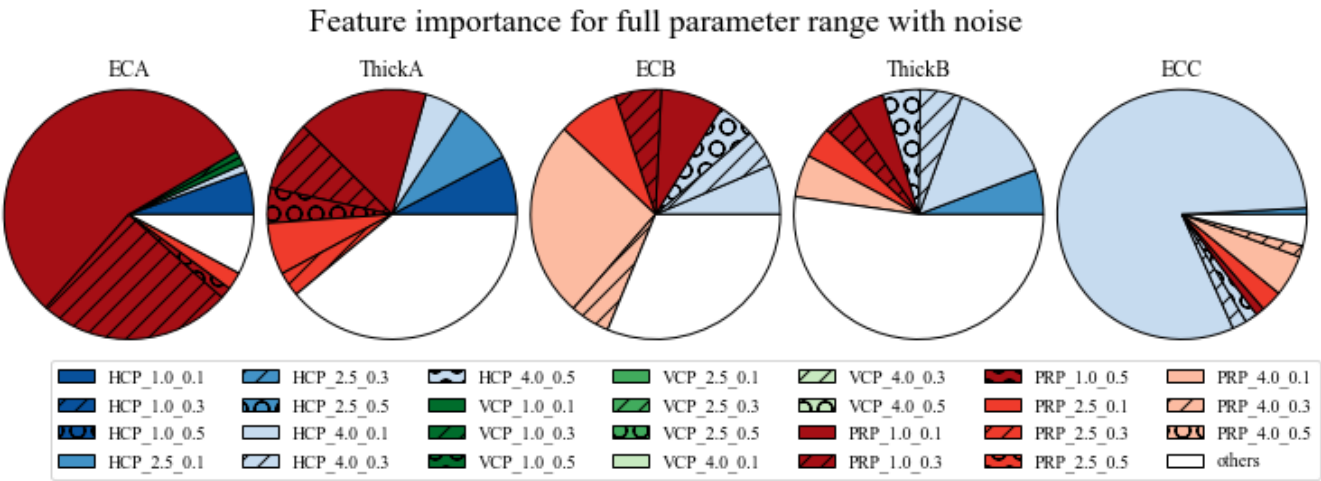
VCP – Vertical co-planar

545

Appendix B The effect of noise on Inferring subsurface parameters and feature importance

To assess the impact of noise 100 realizations of heteroscedastic gaussian noise with a standard deviation of 0.05. The ensemble

from the full solution was multiplied by the random noise prior to ML application to the full ensemble (no restrictions). This

was repeated for each realization of noise and the average fit and their standard deviation are shown in table B1.

550 **Table B1 The root mean square error (RMSE) between the prediction from the gradient boosted (GB) model and the testing data. The machine learning procedure was repeated with each of the five subsurface parameters as targets, thus creating five models.**

Target	ECA	ThickA	ECB	ThickB	ECC
Unit	mS/m	m	mS/m	m	mS/m
RMSE	7.09	0.29	18.8	0.51	2.98
RMSE (noise)	12.4	0.41	23.3	0.58	8.00
Std (noise)	0.05	0.0008	0.05	0.0008	0.02

The average feature importance over the 100 realizations (Fig. B1) affects ThickA, ECB and ThickB the most. Here the feature

importance is distributed more evenly among the configurations compared to without noise.

Feature importance for full parameter range with noise

ECA   ThickA   ECB   ThickB   ECC

▬ HCP_1.0_0.1	▨ HCP_2.5_0.3	◠ HCP_4.0_0.5
▨ HCP_1.0_0.3	▧ HCP_2.5_0.5	▬ VCP_1.0_0.1
▨ HCP_1.0_0.5	▢ HCP_4.0_0.1	▬ VCP_1.0_0.3
▬ HCP_2.5_0.1	▨ HCP_4.0_0.3	◠ VCP_1.0_0.5

▬ VCP_2.5_0.1	▨ VCP_4.0_0.3	▬ PRP_1.0_0.5	▬ PRP_4.0_0.1
▨ VCP_2.5_0.3	▨ VCP_4.0_0.5	▬ PRP_2.5_0.1	▨ PRP_4.0_0.3
◠ VCP_2.5_0.5	▬ PRP_1.0_0.1	▨ PRP_2.5_0.3	▨ PRP_4.0_0.5
▢ VCP_4.0_0.1	▨ PRP_1.0_0.3	◠ PRP_2.5_0.5	▢ others

555

Figure B1 Feature importance for inferring each of the five parameters from a decision tree analysis of the full parameter range. The feature importance from all 27 configurations sum to 1. The eight most important configurations for inferring each of the five parameters are shown with a unique color and pattern combination. The remaining 19 configurations are aggregated into the "others" category and displayed with white

560

Code and data availability

The modelled EMI data and code used in this study is available on https://zenodo.org/record/5745749

Author Contributions

Competing interests

The authors declare that they have no conflict of interest.

Acknowledgements

References

Acworth, R. I. Investigation of dryland salinity using the electrical image method. *Australian Journal of Soil Research*, *37*(4), 623–636. https://doi.org/10.1071/sr98084, 1999.

Adamchuk, V., Allred, B., Doolittle, J., Grote, K., & Viscarra Rossel, R.. *Tools for Proximal Soil Sensing*, 2015.

Adhikari, K., & Hartemink, A. E. Soil organic carbon increases under intensive agriculture in the Central Sands, Wisconsin, USA. *Geoderma Regional*, *10*(August 2016), 115–125. https://doi.org/10.1016/j.geodrs.2017.07.003, 2017.

Anderson, W. L. Numerical integration of related Hankel transforms of orders 0 and 1 by adaptive digital filtering. *Geophysics*, *44*(7), 1287–1305, 1979.

Auken, E., Christiansen, A. V., Kirkegaard, C., Fiandaca, G., Schamper, C., Behroozmand, A. A., … Vignoli, G. An overview of a highly versatile forward and stable inverse algorithm for airborne, ground-based and borehole electromagnetic and electric data. *Exploration Geophysics*, *46*(3), 223–235. https://doi.org/10.1071/EG13097, 2015.

Beamish, D. Low induction number, ground conductivity meters: A correction procedure in the absence of magnetic effects. *Journal of Applied Geophysics*, *75*(2), 244–253. https://doi.org/10.1016/j.jappgeo.2011.07.005, 2011.

Binley, A., Hubbard, S. S., Huisman, J. A., Revil, A., Robinson, D. A., Singha, K., & Slater, L. D. The emergence of hydrogeophysics for improved understanding of subsurface processes over multiple scales. *Water Resources Research*, *51*(6), 3837–3866. https://doi.org/https://doi.org/10.1002/2015WR017016, 2015.

590 Breiman, L. Bagging predictors. *Machine Learning*, *24*(2), 123–140. https://doi.org/10.1007/BF00058655, 1996.

Callegary, J. B., Ferré, T. P. A., & Groom, R. W. Vertical Spatial Sensitivity and Exploration Depth of Low-Induction-Number Electromagnetic-Induction Instruments. *Vadose Zone Journal*, *6*(1), 158–167. https://doi.org/10.2136/vzj2006.0120, 2007.

Callegary, J. B., Ferré, T. P. A., & Groom, R. W. Three-Dimensional Sensitivity Distribution and Sample Volume of Low-595 Induction-Number Electromagnetic-Induction Instruments. *Soil Science Society of America Journal*, *76*(1), 85–91. https://doi.org/10.2136/sssaj2011.0003, 2012.

Christiansen, A. V., Pedersen, J. B., Auken, E., Søe, N. E., Holst, M. K., & Kristiansen, S. M. Improved geoarchaeological mapping with electromagnetic induction instruments from dedicated processing and inversion. *Remote Sensing*, *8*(12). https://doi.org/10.3390/rs8121022, 2016.

600 Cockx, L., Van Meirvenne, M., Vitharana, U. W. A., Verbeke, L. P. C., Simpson, D., Saey, T., & Van Coillie, F. M. B. Extracting Topsoil Information from EM38DD Sensor Data using a Neural Network Approach. *Soil Science Society of America Journal*, *73*(6), 2051. https://doi.org/10.2136/sssaj2008.0277, 2009.

Daccache, A., Knox, J. W., Weatherhead, E. K., Daneshkhah, A., & Hess, T. M. Implementing precision irrigation in a humid climate - Recent experiences and on-going challenges. *Agricultural Water Management*, *147*, 135–143. 605 https://doi.org/10.1016/j.agwat.2014.05.018, 2015.

De Smedt, P., Van Meirvenne, M., Saey, T., Baldwin, E., Gaffney, C., & Gaffney, V. Unveiling the prehistoric landscape at Stonehenge through multi-receiver EMI. *Journal of Archaeological Science*, *50*(1), 16–23. https://doi.org/10.1016/j.jas.2014.06.020, 2014.

Doolittle, J. A., & Brevik, E. C. The use of electromagnetic induction techniques in soils studies. *Geoderma*, *223–225*(1), 33–610 45. https://doi.org/10.1016/j.geoderma.2014.01.027, 2014.

Elith, J., Leathwick, J. R., & Hastie, T. A working guide to boosted regression trees. *Journal of Animal Ecology*, *77*(4), 802–813. https://doi.org/10.1111/j.1365-2656.2008.01390.x, 2008.

Friedman, J. H. Greedy function approximation: A gradient boosting machine. *Ann. Statist.*, *29*(5), 1189–1232. https://doi.org/10.1214/aos/1013203451, 2001.

615 Friedman, J. H., & Meulman, J. J. Multiple additive regression trees with application in epidemiology. *Statistics in Medicine*, *22*(9), 1365–1381. https://doi.org/10.1002/sim.1501, 2003.

Furman, A., Ferré, T. P. A., & Heath, G. L. Spatial focusing of electrical resistivity surveys considering geologic and hydrologic layering. *GEOPHYSICS*, *72*(2), F65–F73. https://doi.org/10.1190/1.2433737, 2007.

Guptasarma, D., & Singh, B. New digital linear filters for Hankel J0 and J1 transforms [link]. *Geophysical Prospecting*, *45*(5), 620 745–762, 1997.

Hanssens, D., Delefortrie, S., Pue, J. De, Meirvenne, M. Van, & Smedt, P. De. Frequency-Domain Electromagnetic Forward and Sensitivity Modeling: Practical Aspects of Modeling a Magnetic Dipole in a Multilayered Half-Space. *IEEE Geoscience and Remote Sensing Magazine*, *7*(1), 74–85. https://doi.org/10.1109/MGRS.2018.2881767, 2019.

Harvey, O. R., & Morgan, C. L. S. Predicting Regional-Scale Soil Variability using a Single Calibrated Apparent Soil Electrical Conductivity Model. *Soil Science Society of America Journal*, *73*(1), 164. https://doi.org/10.2136/sssaj2008.0074, 2009.

Hastie, T., Tibshirani, R., & Friedman, J. *The Elements of Statistical Learning*. New York, NY, USA: Springer New York Inc, 2001.

Heil, K., & Schmidhalter, U. Characterisation of soil texture variability using the apparent soil electrical conductivity at a highly variable site. *Computers and Geosciences*, *39*, 98–110. https://doi.org/10.1016/j.cageo.2011.06.017, 2012.

Heil, K, & Schmidhalter, U. Comparison of the EM38 and EM38-MK2 electromagnetic induction-based sensors for spatial soil analysis at field scale. *COMPUTERS AND ELECTRONICS IN AGRICULTURE*, *110*, 267–280. https://doi.org/10.1016/j.compag.2014.11.014, 2015.

Heil, Kurt, & Schmidhalter, U. The application of EM38: Determination of soil parameters, selection of soil sampling points and use in agriculture and archaeology. *Sensors (Switzerland)*, *17*(11). https://doi.org/10.3390/s17112540, 2017.

Heil, Kurt, & Schmidhalter, U. Theory and Guidelines for the Application of the Geophysical Sensor EM38. *Sensors (Basel, Switzerland)*, *19*(19). https://doi.org/10.3390/s19194293, 2019.

James, I. T., Waine, T. W., Bradley, R. I., Taylor, J. C., & Godwin, R. J. Determination of Soil Type Boundaries using Electromagnetic Induction Scanning Techniques. *Biosystems Engineering*, *86*(4), 421–430. https://doi.org/10.1016/j.biosystemseng.2003.09.001, 2003.

Khodja, M. R., Prange, M. D., & Djikpesse, H. A. Guided Bayesian optimal experimental design. *Inverse Problems*, *26*(5). https://doi.org/10.1088/0266-5611/26/5/055008, 2010.

Mason, L., Baxter, J., Bartlett, P., & Frean, M. Boosting Algorithms as Gradient Descent. *Proceedings of the 12th International Conference on Neural Information Processing Systems*, 512–518. Cambridge, MA, USA: MIT Press, 1999.

McCutcheon, M. C., Farahani, H. J., Stednick, J. D., Buchleiter, G. W., & Green, T. R. Effect of Soil Water on Apparent Soil Electrical Conductivity and Texture Relationships in a Dryland Field. *Biosystems Engineering*, *94*(1), 19–32. https://doi.org/10.1016/j.biosystemseng.2006.01.002, 2006.

McLachlan, P., Blanchy, G., & Binley, A. EMagPy: open-source standalone software for processing, forward modeling and inversion of electromagnetic induction data. *Computers & Geosciences*, 104561. https://doi.org/https://doi.org/10.1016/j.cageo.2020.104561, 2020.

McNeill, J. D. Electromagnetic Terrain Conductivity Measurement at Low Induction Numbers. *Technical Note TN*, Vol. 6, p. 13. Retrieved from http://www.geonics.com/pdfs/technicalnotes/tn6.pdf, 1980.

Monteiro Santos, F. A. 1-D laterally constrained inversion of EM34 profiling data. *Journal of Applied Geophysics*, *56*(2), 123–134. https://doi.org/https://doi.org/10.1016/j.jappgeo.2004.04.005, 2004.

Nabighian, M. N., & Macnae, J. C. 6. Time Domain Electromagnetic Prospecting Methods. In *Investigations in Geophysics*.

655   *Electromagnetic Methods in Applied Geophysics: Volume 2, Application, Parts A and B* (pp. 427–520). https://doi.org/doi:10.1190/1.9781560802686.ch6, 1991.

Nimmo, J. R. Vadose Water. *Encyclopedia of Inland Waters*, *1*, 766–777. https://doi.org/10.1016/B978-012370626-3.00014-4, 2009.

Palacky, G. J. 3. Resistivity Characteristics of Geologic Targets. *Electromagnetic Methods in Applied Geophysics*, 52–129.
660   https://doi.org/10.1190/1.9781560802631.ch3, 2011.

Pedregosa, F., Varoquaux, G., Gramfort, A., Michel, V., Thirion, B., Grisel, O., … Duchesnay, E. Scikit-learn: Machine Learning in {P}ython. *Journal of Machine Learning Research*, *12*, 2825–2830, 2011.

Reyes, J., Wendroth, O., Matocha, C., Zhu, J., Ren, W., & Karathanasis, A. D. Reliably Mapping Clay Content Coregionalized with Electrical Conductivity. *Soil Science Society of America Journal*, *0*(0), 0.
665   https://doi.org/10.2136/sssaj2017.09.0327, 2018.

Robinson, D. A., Abdu, H., Jones, S. B., Seyfried, M., Lebron, I., & Knight, R. Eco-Geophysical Imaging of Watershed-Scale Soil Patterns Links with Plant Community Spatial Patterns. *Vadose Zone Journal*, *7*(4), 1132. https://doi.org/10.2136/vzj2008.0101, 2008.

Saey, T., De Smedt, P., De Clercq, W., Meerschman, E., Monirul Islam, M., & Van Meirvenne, M. Identifying Soil Patterns
670   at Different Spatial Scales with a Multi-Receiver EMI Sensor. *Soil Science Society of America Journal*, *77*(2), 382. https://doi.org/10.2136/sssaj2012.0276, 2013.

Saey, T., Simpson, D., Vermeersch, H., Cockx, L., & Van Meirvenne, M. Comparing the EM38DD and DUALEM-21S Sensors for Depth-to-Clay Mapping. *Soil Science Society of America Journal*, *73*(1), 7–12. https://doi.org/10.2136/sssaj2008.0079, 2009.

675 Saey, T., Van Meirvenne, M., De Smedt, P., Stichelbaut, B., Delefortrie, S., Baldwin, E., & Gaffney, V. Combining EMI and GPR for non-invasive soil sensing at the stonehenge world heritage site: The reconstruction of a WW1 practice trench. *European Journal of Soil Science*, *66*(1), 166–178. https://doi.org/10.1111/ejss.12177, 2015.

Saey, T., Van Meirvenne, M., Vermeersch, H., Ameloot, N., & Cockx, L. A pedotransfer function to evaluate the soil profile textural heterogeneity using proximally sensed apparent electrical conductivity. *Geoderma*, *150*(3–4), 389–395.
680   https://doi.org/10.1016/j.geoderma.2009.02.024, 2009.

Saey, T, De Smedt, P., Islam, M. M., Meerschman, E., Van De Vijver, E., Lehouck, A., & Van Meirvenne, M. Depth slicing of multi-receiver EMI measurements to enhance the delineation of contrasting subsoil features. *Geoderma*, *189–190*, 514–521. https://doi.org/10.1016/j.geoderma.2012.06.010, 2012.

Saey, T, Verhegge, J., Smedt, P. De, Smetryns, M., Note, N., Vijver, E. Van De, … Delefortrie, S. Catena Integrating cone
685   penetration testing into the 1D inversion of multi-receiver EMI data to reconstruct a complex stratigraphic landscape . *Catena*, *147*, 356–371. https://doi.org/10.1016/j.catena.2016.07.023, 2016.

Song, L.-P., Pasion, L. R., Lhomme, N., & Oldenburg, D. W. Sensor Placement via Optimal Experiment Design in EMI Sensing of Metallic Objects. *Mathematical Problems in Engineering*, *2016*, 5856083.

https://doi.org/10.1155/2016/5856083, 2016.

690   Triantafilis, J., & Lesch, S. M. Mapping clay content variation using electromagnetic induction techniques. *Computers and Electronics in Agriculture*, *46*(1-3 SPEC. ISS.), 203–237. https://doi.org/10.1016/j.compag.2004.11.006, 2005.

Von Hebel, C., Van Der Kruk, J., Huisman, J. A., Mester, A., Altdorff, D., Endres, A. L., … Vereecken, H. Calibration, conversion, and quantitative multi-layer inversion of multi-coil rigid-boom electromagnetic induction data. *Sensors (Switzerland)*, *19*(21). https://doi.org/10.3390/s19214753, 2019.

695   Wait, J. *Geo-Electromagnetism*. Academic Press, New York, 1982.

Winter, T. C., Harvey, J. W., Franke, O. L., & Alley, W. M. Ground Water Surface Water and A Single Resource. *USGS Publications*, 79. Retrieved from http://pubs.usgs.gov/circ/circ1139/pdf/circ1139.pdf, 1998.

700